Mechanical Systems and Signal Processing 120 (2019) 290–307

Contents lists available at ScienceDirect

Mechanical Systems and Signal Processing

journal homepage: www.elsevier.com/locate/ymssp

Subsystem identification in structures with a human occupant based on composite frequency response functions

Xiaojun Wei [a,c,*], Stana Živanović [b,c], Justin Russell [c], John E. Mottershead [d]

[a] Department of Mechanical and Vehicle Engineering, Hunan University, Changsha 410082, China
[b] College of Engineering, Mathematics and Physical Sciences, University of Exeter, Exeter EX4 4QF, UK
[c] School of Engineering, University of Warwick, Coventry CV4 7AL, UK
[d] Department of Mechanical, Materials and Aerospace Engineering, University of Liverpool, Liverpool L69 3GH, UK

ARTICLE INFO

Article history:
Received 31 March 2018
Received in revised form 25 July 2018
Accepted 15 September 2018
Available online 29 October 2018

Keywords:
Human-structure interaction
Subsystem identification
Impact hammer testing
Frequency response function

ABSTRACT

A method is proposed for the subsystem identification of a composite system composing a lightweight low-frequency civil engineering structure and a human occupant. It is shown for the first time that the dynamics of the structure and the stiffness and damping of the human occupant can be determined from the frequency response functions of the composite system and the known mass of the human occupant. The advantage of the proposed approach over existing methods is not only in the simplicity of problem formulation but also in the substantial reduction of experimental complexity. Subsystem identification is demonstrated using a numerical example and two experimental case studies. In the first experimental case study, the method is applied to a laboratory bridge with a human occupant in a standing posture and frequency response functions are measured using shaker testing. In the second case study, the method is applied to a laboratory bridge with a hammer operator crouching on the bridge to perform impact hammer tests. It is demonstrated that subsystem dynamics can be accurately identified. The method is especially applicable to the correction of the effect of the hammer operator in manually operated impact hammer testing. In addition, the method can be generalised for the compenstation of the effects of the electrodynamic shaker in shaker testing for civil engineering applications.

1. Introduction

Human-structure interaction is a well-recognised phenomenon which involves the interplay of the dynamics of the two subsystems in human-structure systems, i.e. the human occupant(s) and the structure supporting the human occupant(s). This mechanism can lead to various modifications of the dynamic properties of the structure, including the increase [1,2] or decrease [1–4] of natural frequencies, increase [1–4] or decrease [2] of damping ratios, and even the appearance of new modes [1,2]. The actual change of dynamic properties and the extent of human-structure interaction are dependent upon the mass, damping and frequency ratios between the occupant(s) and the structure [2,5].

The effect of human-structure interaction has become of major importance in vibration serviceability design of lightweight and slender structures in the last two decades [1,6–9]. In structural design applications, the dynamics of the human body are commonly represented by a single degree of freedom (SDOF) mass-spring-damper model [10–18]. The research

* Corresponding author at: Department of Mechanical and Vehicle Engineering, Hunan University, Changsha 410082, China.
E-mail address: x.wei.3@warwick.ac.uk (X. Wei).

https://doi.org/10.1016/j.ymssp.2018.09.018
0888-3270/

mainly concerns identifying human body dynamics [10–18] and predicting the dynamics of human-structure systems [5,18–22]. The human body dynamics may be identified directly by curve fitting measured driving-point apparent masses [11,12] or derived indirectly from the known dynamics of the empty structure and the human-structure system [10,13–18]. When the dynamics of the human occupant and the empty structure are known, the dynamic prediction of the joint system is relatively straightforward. Specifically, a spatial or modal model of the joint system is first constructed by combining the known spatial or modal model of the empty structure and the human model, based on which the dynamic prediction is performed.

Manually operated impact hammer testing is another structural engineering application which involves human-structure interaction. It has been widely utilised for modal analysis of small and medium civil engineering structures thanks to its convenience, efficiency and economy [23,24]. For such testing, a hammer operator is present on the structure during the data collection. Consequently, the identified dynamic properties are essentially those of the human-structure system rather than those of the empty structure. For some lightweight low-frequency structures, especially with frequencies close to the frequency of the human body, the influence of the human occupant can be significant [18,25]. Unfortunately, existing system identification methods using data from impact hammer tests routinely neglect the effect of the hammer operator, which might lead to significant errors in the dynamic identification of the empty structure. Little attention has been paid to the elimination of the effect of the hammer operator in impact hammer testing. Recently, Wei and Živanović [18] stressed the importance of the effect of the hammer operator on the dynamic identification of the empty structure and presented explicit formulas for deriving the frequency response functions (FRFs) of the empty structure provided that the human body dynamics and the measured FRFs of the human-structure system are both known. In addition, other methods for identifying human body dynamics [13–16] could also be used for the dynamic identification of the empty structure if the dynamics of the human body and the human-structure system are both known. However, the aforementioned methods [13–16,18] require the identification of the dynamics of the particular hammer operator from laboratory experiments, in which the hammer operator should keep the same posture as that employed in the on-site impact hammer tests. An alternative might be to adopt existing human-body models from the literature, but this introduces errors due to inter- and intra-subject variations [11,15,26,27].

This paper proposes a new method for identifying the dynamics of the human body and the empty structure in a human-structure system, based only on the measured FRFs of the composite system. A pair of eigenvalues of the empty structure are first identified using three measured direct FRFs of the structure with a human occupant at three different locations. In the next step, the human body dynamics are explicitly derived in terms of the identified eigenvalues of the empty structure and FRFs of the human-structure system. Finally, the FRFs of the empty structure are explicitly deduced in terms of the FRFs of the human-structure system and the identified human body dynamics. Therefore, the proposed method is superior to the existing methods for identifying human body dynamics [10,13–18] which require knowledge of both the dynamics of the empty structure and the human-structure system. In addition, the proposed method is superior to the existing methods for identifying the dynamics of the empty structure which require knowledge of the human body dynamics, typically obtained from separate laboratory experiments, and the dynamics of the human-structure system. The separate laboratory experiments for identifying human body dynamics require either a lightweight low-frequency structure by the indirect method [10,13–18], or a shaker and a force platform directly [11]. The necessary equipment may not be available to industrial engineers and even to researchers. The proposed method, requiring only on-site experiments for obtaining the FRFs of the structure occupied by a human occupant, is more economical than existing methods and avoids the effects of the inter- and intra-subject variations caused by adopting standard human-body dynamic models from literature. The proposed method is especially applicable to the elimination of the effect of the hammer operator in manually operated impact hammer testing. Additionally, this approach can be generalised to correct the effects of the electrodynamic shaker in shaker testing. Furthermore, this paper discusses the effects of the time delay between the response and force signal measurement on measured FRFs of the structure under test and proposes appropriate strategies for correcting these effects. This paper concerns a single human occupant interaction with lightweight low-frequency structures (i.e. vibration modes with natural frequencies up to about 8 Hz) with well-sperated modes. In this frequency region, the first vibration mode of the human occupant is likely to interact with the structure, and therefore the human body is modelled as a SDOF system. The effect of the uncertainty in human body dynamics on the dynamic identification of the empty structure can be investigated using the perturbation method presented in the paper [18], therefore it is not elaborated here.

Following this introductory section, Section 2 introduces the theory for the identification of the dynamics of the human body and the empty structure in a human-structure system. A numerical illustration of the working of the method is presented in Section 3, whilst its experimental demonstrations are presented in Section 4. Conclusions are drawn in Section 5.

2. Theory

This section presents the theory for the identification of the dynamics of both the human body and the empty structure from the measured FRFs of a human-structure system.

2.1. The relationship between the FRFs of the empty structure and the human-structure system

The dynamics of a linear structure having n DOFs are modified when occupied by a stationary human. The SDOF dynamics of the human body are represented by mass m_h, damping c_h and stiffness k_h. m_h is assumed to represent the physical mass of

the human body in line with some previous studies [3,10,18,28–31]. Therefore, the presence of the human occupant introduces an additional DOF, denoted as the $(n+1)$-th DOF. Without loss of generality, it is assumed that the human occupant is located at the p-th DOF ($p \le n$) of the structure. The stiffness and damping elements of the human body are connecting the p-th and $(n+1)$-th DOFs and the mass of the human body is considered to be concentrated at the $(n+1)$-th DOF.

Wei and Živanović [18] showed that the direct receptance at the p-th DOF of the empty structure $h_{pp}^{s}(s)$ and that of the human-structure system $h_{pp}^{sh,p}(s)$, where s is the Laplace variable and p in the superscript indicates the location of the human occupant, may be expressed as

$$h_{pp}^{s}(s) = \frac{\left(1+\frac{1}{m_h s^2}(c_h s + k_h)\right) h_{pp}^{sh,p}(s)}{1+\frac{1}{m_h s^2}(c_h s + k_h) - (c_h s + k_h) h_{pp}^{sh,p}(s)} \tag{1}$$

and the cross receptance between the q-th DOF ($q \le n$) and the p-th DOF of the empty structure $h_{qp}^{s}(s)$ and that of the human-structure system $h_{qp}^{sh,p}(s)$ are given by

$$h_{qp}^{s}(s) = h_{qp}^{sh,p}(s) + \frac{h_{qp}^{sh,p}(s)(c_h s + k_h) h_{pp}^{sh,p}(s)}{1+\frac{1}{m_h s^2}(c_h s + k_h) - (c_h s + k_h) h_{pp}^{sh,p}(s)} \tag{2}$$

2.2. Identification of a pair of eigenvalues of the empty structure

The denominator of Eqs. (1) or (2) generates the characteristic equation

$$1+\frac{1}{m_h \mu_i^2}(c_h \mu_i + k_h) - (c_h \mu_i + k_h) h_{pp}^{sh,p}(\mu_i) = 0 \tag{3}$$

where μ_i is the i-th eigenvalue corresponding the i-th mode of the empty structure.

Similarly, if the human occupant is located at the q-th DOF of the structure, then

$$1+\frac{1}{m_h \mu_i^2}(c_h \mu_i + k_h) - (c_h \mu_i + k_h) h_{qq}^{sh,q}(\mu_i) = 0 \tag{4}$$

where $h_{qq}^{sh,q}(s)$ is the direct receptance at the q-th DOF of the structure with the human occupant at the q-th DOF.

Subtracting Eq. (4) from Eq. (3) leads to

$$(c_h \mu_i + k_h)\left(h_{qq}^{sh,q}(\mu_i) - h_{pp}^{sh,p}(\mu_i)\right) = 0 \tag{5}$$

Since the eigenvalues of an actual underdamped stable structure are complex,

$$(c_h \mu_i + k_h) \neq 0 \tag{6}$$

Therefore, Eq. (5) is equivalent to

$$h_{qq}^{sh,q}(\mu_i) - h_{pp}^{sh,p}(\mu_i) = 0 \tag{7}$$

which indicates that the eigenvalues of the empty structure are zeros of the rational function

$$\Delta h^{qp}(s) = h_{qq}^{sh,q}(s) - h_{pp}^{sh,p}(s) = 0. \tag{8}$$

However, $\Delta h^{qp}(s)$ generally has additional zeros that are not related to the dynamics of the empty structure. The selection of correct eigenvalues for the empty structure requires additional checks.

Due to relatively small changes of the human-structure system properties compared to the properties of the empty structure, the eigenvalues of any particular mode of the empty structure will be close to those of the corresponding mode of the human-structure system. Let us assume that the i - th pair of complex conjugate eigenvalues μ_i^s and $\bar{\mu}_i^s$ of the empty structure are the targets for identification. The i - th pair of complex conjugate eigenvalues μ_i^{sh} and $\bar{\mu}_i^{sh}$, corresponding to the i - th mode dominated by the structural motion of the human-structure system, should be good initial guesses for μ_i^s and $\bar{\mu}_i^s$, respectively, when solving Eq. (8) by using algorithms for solving nonlinear equations, e.g. the trust region algorithm [32]. In the frequency range around the i-th mode dominated by the structural motion of the human-structure system, the FRF curves of $h_{qq}^{sh,q}(s)$ and $h_{pp}^{sh,p}(s)$ have at most three intersections nearest to their peaks (under the assumption that vibration modes of the empty structure are well sperated). The zeros of $\Delta h^{qp}(s)$ related to the dynamics of the empty structure can be checked since the correct eigenvalues of the empty structure should also be the zeros of $\Delta h^{rp}(s) = h_{rr}^{sh,r}(s) - h_{pp}^{sh,p}(s)$ and

$\Delta h^{rq}(s) = h_{rr}^{sh,r}(s) - h_{qq}^{sh,q}(s)$ where $h_{rr}^{sh,r}(s)$ is the measured direct receptance at the r-th DOF of the human-structure system with the human occupant at the r-th DOF.

2.3. Identification of the dynamics of the human body

Let us assume that the eigenvalues μ_i^s and $\bar{\mu}_i^s$ of the empty structure have been identified by the proposed approach described in Section 2.2. The eigenvalues μ_i^s and $\bar{\mu}_i^s$ should satisfy Eq. (3), i.e.

$$\begin{bmatrix} c_h \\ k_h \end{bmatrix} = \begin{bmatrix} \mu_i^s & 1 \\ \bar{\mu}_i^s & 1 \end{bmatrix}^{-1} \begin{bmatrix} \dfrac{(\mu_i^s)^2 m_h}{(\mu_i^s)^2 m_h h_{pp}^{sh,p}(\mu_i^s) - 1} \\ \dfrac{(\bar{\mu}_i^s)^2 m_h}{(\bar{\mu}_i^s)^2 m_h h_{pp}^{sh,p}(\bar{\mu}_i^s) - 1} \end{bmatrix} \tag{9}$$

Eq. (9) infers that the damping c_h and stiffness k_h of the human body can be calculated using the mass m_h of the human body and the direct receptance of the human-structure system $h_{pp}^{sh,p}(s)$ evaluated at a pair of eigenvalues μ_i^s and $\bar{\mu}_i^s$ of the empty structure. Eq. (9) always results in real solutions for c_h and k_h due to the use of the complex conjugate pair μ_i^s and $\bar{\mu}_i^s$.

If the measured quantity is accelerance rather than receptance, an alternative form of Eq.(9) should be used. It is known that the acceleration $\boldsymbol{a}(s)$ and the displacement $\boldsymbol{x}(s)$ are related by $\boldsymbol{a}(s) = s^2\boldsymbol{x}(s)$. The receptance matrix $\boldsymbol{H}^{sh}(s)$ and the accelerance matrix $\boldsymbol{H}_a^{sh}(s)$ satisfy the relationship

$$\boldsymbol{H}^{sh}(s) = \frac{\boldsymbol{H}_a^{sh}(s)}{s^2} \tag{10}$$

leading to the estimate of the damping and stiffness of the human from Eq. (11)

$$\begin{bmatrix} c_h \\ k_h \end{bmatrix} = \begin{bmatrix} \mu_i^s & 1 \\ \bar{\mu}_i^s & 1 \end{bmatrix}^{-1} \begin{bmatrix} \dfrac{(\mu_i^s)^2 m_h}{m_h h_{a,pp}^{sh,p}(\mu_i^s) - 1} \\ \dfrac{(\bar{\mu}_i^s)^2 m_h}{m_h h_{a,pp}^{sh,p}(\bar{\mu}_i^s) - 1} \end{bmatrix} \tag{11}$$

Note that the same human body dynamics will be identified if any other direct receptance (e.g. $h_{qq}^{sh,q}$ or $h_{rr}^{sh,r}$) of the human-structure system is used in Eq. (9) because they are equal to each other at the eigenvalues of the empty structure.

2.4. Identification of the dynamics of the empty structure

The direct and cross receptances of the empty structure can be calculated using Eqs. (1) and (2), the human body dynamics and the direct and cross receptances of the human-structure system. The frequencies and damping ratios can then be obtained by solving the characteristic equation of the receptances of the empty structure. Since the human body dynamics can be identified from measured direct receptances of the human-structure system, the dynamics of the empty structure can be obtained entirely from measured direct and cross receptances of the human-structure system.

3. Numerical example

A numerical example was conducted based on an actual glass fibre reinforced polymer simply supported bridge [25]. A schematic of the bridge is shown in Fig. 1. The bridge model has a span of $L = 16.9$ m, density $\rho = 1.9 \times 10^3$ kg·m^{-3}, area of cross section $A = 4.89 \times 10^{-2}$ m^2, longitudinal modulus of elasticity $E = 2.47 \times 10^{10}$ N·m^{-2}, second moment of area $I = 3.5 \times 10^{-3}$ m^4, shear modulus $G = 3.9 \times 10^9$ N·m^{-2} and shear coefficient $\kappa = 0.08$. A human occupant having mass

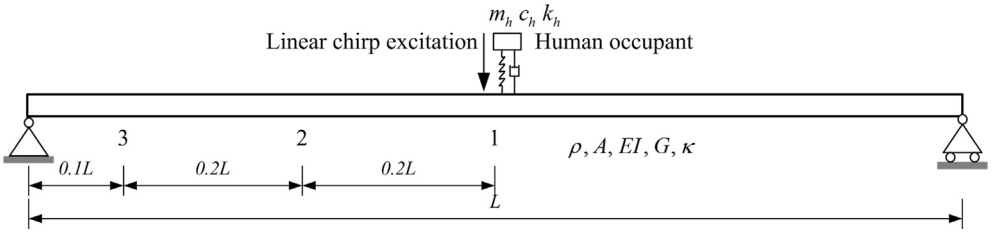

Fig. 1. A schematic of a simply supported bridge with a human occupant and a linear chirp excitation at point 1.

$m_h = 62$ kg, natural frequency $f_h = 5.0$ Hz and damping ratio $\zeta_h = 37.0\%$, corresponding to the human model for standing posture specified in ISO 5982 [33], is assumed to stand on the bridge. The bridge systems with the human occupant located at points 1, 2 and 3 are designated as the systems SH1, SH2 and SH3, respectively.

A two-dimensional finite element (FE) model of the bridge was developed using an improved two-node Timoshenko beam finite element [34]. The FE model consisted of 120 elements of equal length. Proportional damping $\boldsymbol{C} = \alpha\boldsymbol{M} + \beta\boldsymbol{K}$ ($\alpha = \beta = 0.0008$) was assumed. Similarly, the FE models of the systems SH1, SH2 and SH3 were constructed.

The four FE models were first used for eigenvalue analysis, which generated the modal parameters of the corresponding actual systems. The natural frequencies and damping ratios of the first mode dominated by structural motion are summarised in Table 1. It is shown that while the relative differences of frequencies of the systems SH1, SH2 and SH3 with respect to the fundamental frequency of the empty bridge are −5.4%, −3.3% and −0.4%, respectively, the counterparts of the damping ratios are 392%, 267% and 33%, respectively. It can be seen that the presence of the human occupant can significantly modify the dynamics of the empty bridge and its effect depends upon the human occupant location.

Based on the FE model, the time-domain responses were numerically calculated for the empty bridge driven by a linear chirp excitation force (having magnitude 100 N and sweeping from 1 Hz to 10 Hz) at point 1 for 112 s (s) and then left to return to rest over the next 8 s. The actual direct receptance $h_{11}^{s}(s)$ of the empty bridge was then calculated using the excitation force and the resultant vertical displacement response at point 1. Similarly, the direct receptances of the systems SH1, SH2 and SH3, i.e. $h_{11}^{sh,1}(s)$, $h_{22}^{sh,2}(s)$ and $h_{33}^{sh,3}(s)$, were calculated. In this example, the direct receptances $h_{11}^{sh,1}(s)$, $h_{22}^{sh,2}(s)$ and $h_{33}^{sh,3}(s)$ play the role of known (usually by measurement) FRFs of the systems SH1, SH2 and SH3. These three actual receptances (abbreviated to 'Act' in Fig. 2) are depicted by the thick solid line, thin dash-dotted line and thick dashed line in Fig. 2, respectively. They exhibit different peak frequencies due to the presence of the human occupant at different locations.

The following demonstrates how to identify the subsystem dynamics from the known receptances $h_{11}^{sh,1}(s)$, $h_{22}^{sh,2}(s)$ and $h_{33}^{sh,3}(s)$. $h_{11}^{sh,1}(s)$ was curve fitted in the frequency range from 3 Hz to 7 Hz using the rational fraction polynomial method [35], which resulted in an analytical expression

$$h_{11}^{sh,1} = \frac{a_0 s^6 + a_1 s^5 + a_2 s^4 + a_3 s^3 + a_4 s^2 + a_5 s + a_6}{b_0 s^2 + b_1 s + b_2} \tag{12}$$

where $a_0 = 2.7933 \times 10^{-12}$ s^4, $a_1 = -5.2539 \times 10^{-11}$ s^3, $a_2 = 6.5769 \times 10^{-9}$ s^2, $a_3 = -1.9874 \times 10^{-8}$ s, $a_4 = 6.3407 \times 10^{-7}$, $a_5 = 1.7085 \times 10^{-4}$ s^{-1}, $a_6 = 0.0277$ s^{-2}, $b_0 = 24.1786$ N·s^2·m^{-1}, $b_1 = 82.3920$ N·s·m^{-1} and $b_2 = 2.0072 \times 10^4$ N·m^{-1}. It should be noted that the rational expression of $h_{11}^{sh,1}(s)$ shown in Eq. (12) is improper and cannot be state-space realisable. Extra numerator polynomial terms in Eq. (12) are used for the compensation of the residual effects of out-of-band modes

Table 1
Modal parameters of the first structural motion dominated mode.

System	Frequency (Hz)	Damping ratio (%)	Relative difference (%)	
			Frequency	Damping ratio
Empty bridge	4.85	1.2	/	/
SH1	4.59	5.9	−5.4	392
SH2	4.69	4.4	−3.3	267
SH3	4.83	1.6	−0.4	33

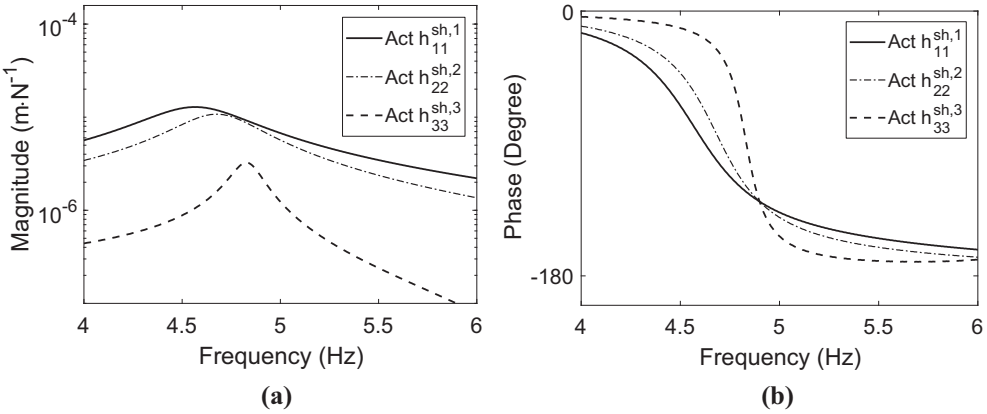

Fig. 2. Direct receptances $h_{11}^{sh,1}(s)$, $h_{22}^{sh,2}(s)$ and $h_{33}^{sh,3}(s)$: (a) Magnitude, (b) Phase.

such that a good fit is achieved. More information about the use of this technique in modal parameter identification applications can be found elsewhere [35]. Its characteristic equation generated the eigenvalue pair $\mu_{1,2}^{sh,1} = -1.7038 \pm 28.7617\mathrm{i}\ \mathrm{s}^{-1}$ for the first mode dominated by the structural motion of the system SH1. The analytical expressions for $h_{22}^{sh,2}(s)$ and $h_{33}^{sh,3}(s)$ were obtained by the same method. Using $\mu_{1,2}^{sh,1}$ as the initial guesses, a pair of eigenvalues of the empty bridge was identified as $\mu_{1,2}^{s} = -0.3735 \pm 30.4551\mathrm{i}\ \mathrm{s}^{-1}$, i.e. the roots $s = \mu_{1,2}^{s}$ of the function

$$\Delta h^{13}(s) = h_{11}^{sh,1}(s) - h_{33}^{sh,3}(s) = 0 \tag{13}$$

$\mu_{1,2}^{s}$ were also found to be the zeros of $\Delta h^{23}(s)$ and $\Delta h^{12}(s)$, which confirms $\mu_{1,2}^{s}$ were the eigenvalues of the empty structure. The corresponding natural frequency and damping ratio were then calculated to be 4.85 Hz and 1.2%, which agree with the actual modal parameters of the empty bridge given in Table 1. While the magnitude curves of $h_{11}^{sh,1}(s)$, $h_{22}^{sh,2}(s)$ and$h_{33}^{sh,3}(s)$, shown in Fig. 2(a), do not exhibit their intersections at $\mu_{1,2}^{s}$ because the intersections are located away from the imaginary axis, their phase curves, shown in Fig. 2(b), indicate the intersections.

In addition, the initial guesses for the solultions to Eq. (13) can be predicted graphically. Fig. 3 shows the contour map of the magnitude of $\Delta h^{13}(s)$ against frequency and damping ratio, which indicates that values around 4.85 Hz and 1.2% are good initial guesses for the frequency and damping ratio of the empty structure, respectively, around which $\Delta h^{13}(s)$ is at its minimum. Note that such a contour map is suggested to be plotted around the eigenvalues of the human-structure system since the eigenvalues of any particular mode of the empty structure will be close to those of the corresponding mode of the human-structure system.

Based on the human body mass, $m_h = 62$ kg, the analytical expression $h_{11}^{sh,1}(s)$ described by Eq. (12) and the identified eigenvalues $\mu_{1,2}^{s}$ of the empty bridge, the damping and stiffness of the human body were calculated as

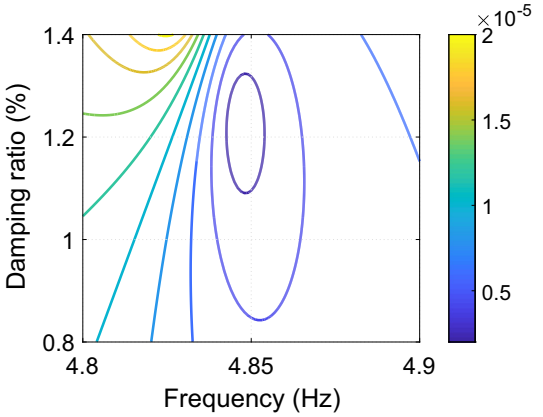

Fig. 3. The magnitude of $\Delta h^{13}(s)$ against frequency and damping ratio.

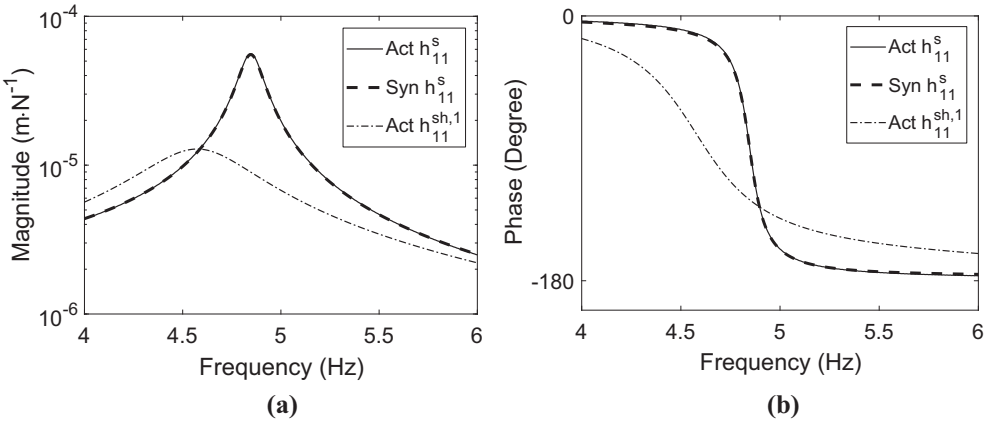

Fig. 4. Direct receptances of SH1 and the empty structure: (a) Magnitude, (b) Phase.

$$\begin{bmatrix} c_h \\ k_h \end{bmatrix} = \begin{bmatrix} \mu_1^s & 1 \\ \mu_2^s & 1 \end{bmatrix}^{-1} \begin{bmatrix} \dfrac{(\mu_1^s)^2 m_h}{(\mu_1^s)^2 m_h h_{11}^{sh,1}(\mu_1^s)-1} \\ \dfrac{(\mu_2^s)^2 m_h}{(\mu_2^s)^2 m_h h_{11}^{sh,1}(\mu_2^s)-1} \end{bmatrix} = \begin{bmatrix} 1.47 \times 10^3 \ \mathrm{N \cdot s \cdot m^{-1}} \\ 6.14 \times 10^4 \ \mathrm{N \cdot m^{-1}} \end{bmatrix}$$

The corresponding frequency and damping ratio of the human body were then calculated as $f_h = 5.0$ Hz and $\zeta_h = 37.0\%$, which are exactly the properties of the actual human occupant stated at the outset.

The direct receptance at point 1 of the empty bridge was then synthesised using Eq. (1), denoted as Syn $h_{11}^s(s)$ and shown by the thick dashed curve in Fig. 4. The synthesised receptance is in good agreement with its actual counterpart (abbreviated to 'Act' and depicted by the thin solid curve in Fig. 4). By solving the characteristic equation for Syn $h_{11}^s(s)$ the fundamental frequency and damping ratio of the empty bridge were found to be 4.85 Hz and 1.2%, which agree with the actual counterparts of the empty bridge. Similarly, the receptances $h_{22}^s(s)$ and $h_{33}^s(s)$ of the empty structure were also obtained. The three direct receptances of the empty structure exhibited the same peak frequency after the elimination of the effect of the human occupant.

4. Experimental case studies

This section presents two experiments for verifying the theory of subsystem identification. The first experiment aims to identify the dynamics of the subsystems of a steel-concrete composite bridge with a human occupant in a standing posture. In this experiment, FRFs were measured by using shaker testing. The second experiment demonstrates how to eliminate the effect of the hammer operator in manually operated impact hammer testing performed on the same bridge. The experiments were approved by the Biomedical and Scientific Research Ethics Committee at the University of Warwick.

4.1. Subsystem identification using measured FRFs from shaker testing

A steel-concrete composite bridge situated in the Structures Laboratory at the University of Warwick (Fig. 5) with a human occupant in a standing posture was considered for subsystem identification. The bridge is 19.9 m long and 2 m wide and sits on two meccano frames with 1.78 m overhang at each end. The bridge and the human occupant weigh 16,500 kg and 100 kg, respectively.

4.1.1. Shaker testing

The accelerances of the empty bridge and the human-bridge system were measured using shaker testing. The test points (TPs) are shown in Fig. 6. An electrodynamic shaker of mass 105.5 kg (Model APS 400), as shown in Fig. 5, was placed sequentially at TPs 1, 2 and 3 on the deck to excite the bridge. The generated force was indirectly measured using an accelerometer (Honeywell QA750, nominal sensitivity 1300 mV/g) attached to the moving armature. Another three accelerometers of the same type were placed at TPs 1, 2 and 3 to measure the vibration responses of the unoccupied bridge and the human-bridge systems in the vertical direction. The data acquisition system consisted of a laptop, a 16-channel data logger (SignalCalc Mobilyser by Data Physics), a signal conditioner and a power amplifier (Model APS 145). A chirp excitation force in the frequency range 1–9 Hz was applied to the structure for 64 s. A data acquisition window was set to 128 s. The sampling frequency was 512 Hz. Four averages were used to minimise the effects of noise. No window was used since the vibration responses returned to the ambient vibration level at the end of the acquisition window. The typical standing posture of the human is shown in Fig. 7.

The bridge systems with the exciter (shaker) located at TPs 1, 2 and 3 are designated as the systems SE1, SE2 and SE3, respectively. The bridge systems with the human occupant and the shaker at TPs 1, 2 and 3 are designated as the systems

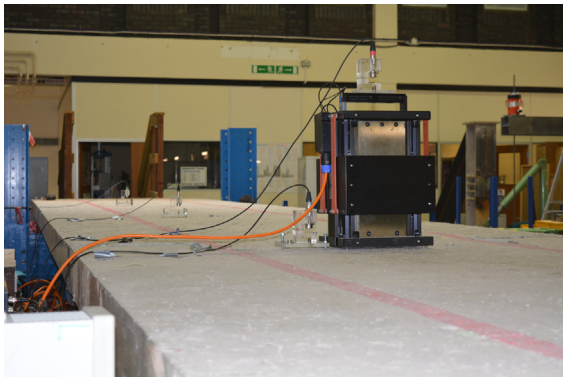

Fig. 5. The bridge with the shaker at TP1.

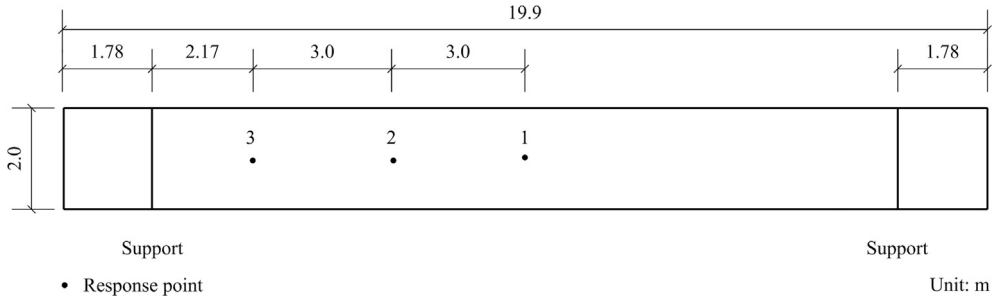

Fig. 6. Bridge deck geometry and test points.

Fig. 7. The bridge with the shaker and the human occupant at TP1.

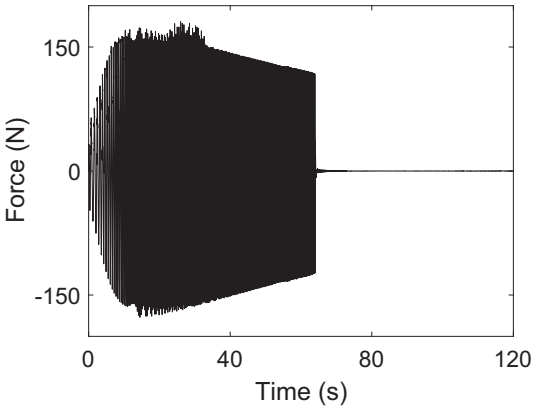

Fig. 8. Excitation force at TP2 of SHE2.

SHE1, SHE2 and SHE3, respectively. The bridge systems with the human occupant at TPs 1, 2 and 3 are designated as the systems SH1, SH2 and SH3, respectively.

The systems SE1, SE2, SE3, SHE1, SHE2 and SHE3 were excited at three different force levels. The maximum accelerations at TP1 of SE1, TP2 of SE2 and TP3 of SE3 ranged from 0.30 $m{\cdot}s^{-2}$ to 0.70 $m{\cdot}s^{-2}$, from 0.22 $m{\cdot}s^{-2}$ to 0.50 $m{\cdot}s^{-2}$ and from 0.14 $m{\cdot}s^{-2}$ to 0.32 $m{\cdot}s^{-2}$, respectively. The maximum accelerations at TP1 of SHE1, TP2 of SHE2 and TP3 of SHE3 ranged from 0.27 $m{\cdot}s^{-2}$ to 0.68 $m{\cdot}s^{-2}$, from 0.21 $m{\cdot}s^{-2}$ to 0.49 $m{\cdot}s^{-2}$ and from 0.13 $m{\cdot}s^{-2}$ to 0.28 $m{\cdot}s^{-2}$, respectively. The frequencies and damping ratios of SE1 showed negligible variation with the response level. The same conclusion was drawn for SE2, SE3, SHE1, SHE2 and SHE3. These findings suggest that the systems SE1, SE2, SE3, SHE1, SHE2 and SHE3 exhibited linear behaviour in the observed amplitude range. Therefore, it is reasonable to assume that the human body exhibited linear behaviour during the testing as well. The force level when excited at TP2 of SHE2 chosen for presentation in this paper is shown in Fig. 8 whilst the corresponding vibration response at TP2 is shown in Fig. 9.

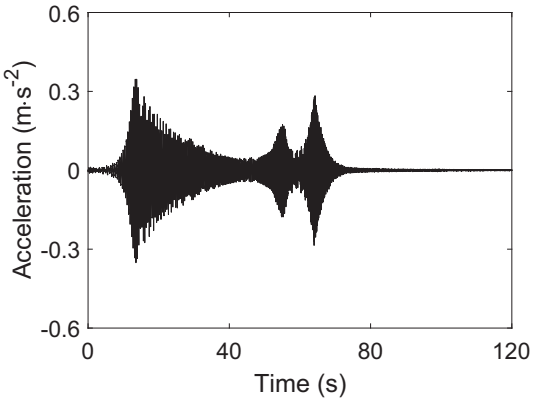

Fig. 9. Acceleration at TP2 of SHE2.

While the direct accelerances at TP1 of SE1, TP2 of SE2 and TP3 of SE3, denoted as $h_{a,11}^{se,1}$, $h_{a,22}^{se,2}$ and $h_{a,33}^{se,3}$, respectively, are shown in Fig. 10, the cross accelerances of SE1, excited at TP1 and measured at TP3, and of SE3, excited at TP3 and measured at TP1, denoted as $h_{a,31}^{se,1}$ and $h_{a,13}^{se,3}$, respectively, are shown in Fig. 11. The direct accelerances at TP1 of SHE1, TP2 of SHE2 and TP3 of SHE3, denoted as $h_{a,11}^{she,1}$, $h_{a,22}^{she,2}$ and $h_{a,33}^{she,3}$ respectively, are shown in Fig. 12. Figs. 10 and 11 show that the presence of the shaker on the deck slightly modifies the dynamics of the bridge under test, i.e. it shifts the natural frequency and affects the reciprocity check. Therefore, the effect of the shaker should be first eliminated from the measured accelerences shown in Fig. 12 before they are used to identify the dynamics of the human body and the empty bridge.

4.1.2. The elimination of the effect of the electrodynamic shaker

The electrodynamic shaker concentrates the majority of its mass on its base (79 kg), while the moving mass is only 26.5 kg. In this research, the shaker is modelled as a mass block of 105.5 kg. By using Eqs. (21) and (22) from Appendix A, the effect of the shaker on the measured accelerences of the empty bridge can be eliminated. Fig. 13 shows the corrected cross accelerances $h_{a,31}^{s}$ (thin solid curve) and $h_{a,13}^{s}$ (thick dashed curve) of the empty bridge, which indicate that the principle of reciprocity is now satisfied. In addition, the natural frequency and damping ratio identified from the corrected accelerances of the empty bridge agree well with the measured counterparts from impact hammer testing in which the hammer operator stood next to the bridge.

Similarly, the effect of the shaker embedded in the measured accelerances $h_{a,11}^{she,1}$, $h_{a,22}^{she,2}$, $h_{a,33}^{she,3}$, $h_{a,31}^{she,1}$ and $h_{a,13}^{she,3}$ can be eliminated. For instance, the measured accelerance of SHE1 $h_{a,11}^{she,1}$ was first curve fitted using the rational fraction polynomial method [35]. Good agreement between the curve-fitted accelerance (thick dashed curve) and its measured counterpart (thin solid curve) is demonstrated in Fig. 14. The analytical expression of the curve-fitted accelerance is

$$h_{a,11}^{she,1}(s) = \frac{a_0 s^2 + a_1 s + a_2}{b_0 s^2 + b_1 s + b_2} \tag{14}$$

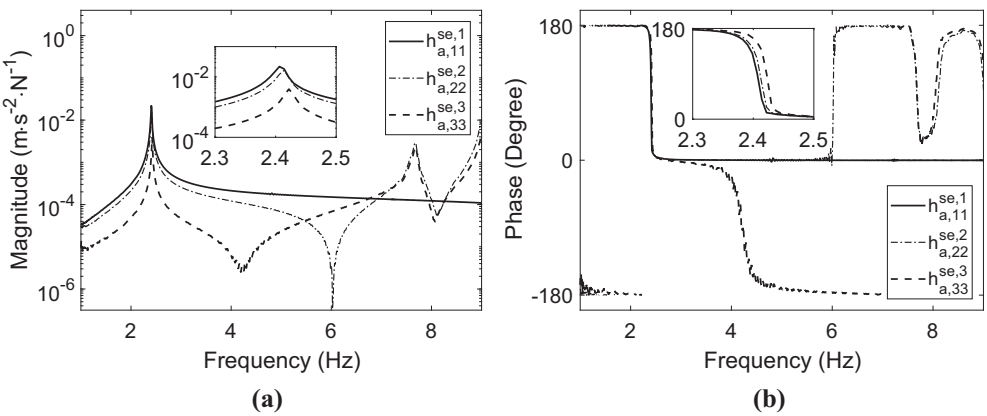

Fig. 10. Measured direct accelerances of the bridge with shaker: (a) Magnitude; (b) Phase.

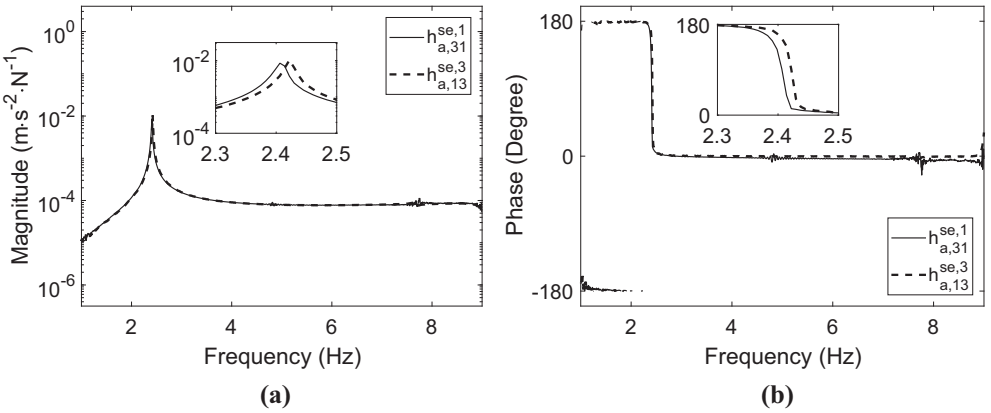

Fig. 11. Measured cross accelerances of the bridge with shaker: (a) Magnitude; (b) Phase.

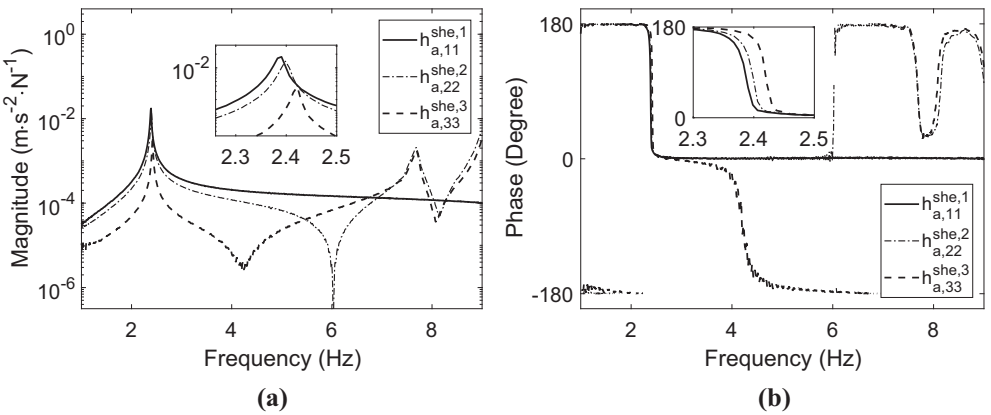

Fig. 12. Measured direct accelerances of the bridge with human occupant and shaker: (a) Magnitude; (b) Phase.

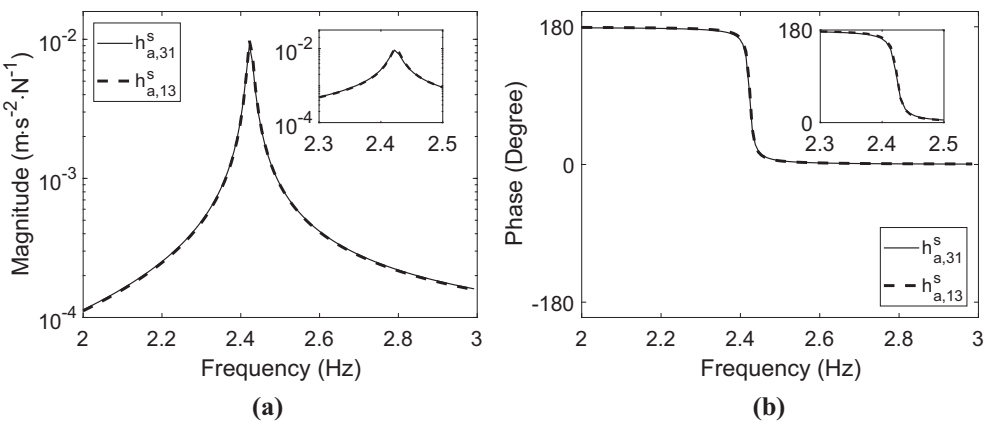

Fig. 13. Corrected cross accelerances of the empty bridge: (a) Magnitude; (b) Phase.

where $a_0 = 2.4738 \times 10^{-4}$, $a_1 = -1.2842 \times 10^{-5}\ \mathrm{s}^{-1}$, $a_2 = -1.6082 \times 10^{-5}\ \mathrm{s}^{-2}$, $b_0 = 1.8417\ \mathrm{N{\cdot}s^2{\cdot}m^{-1}}$, $b_1 = 0.1967\ \mathrm{N{\cdot}s{\cdot}m^{-1}}$ and $b_2 = 413.4934\ \mathrm{N{\cdot}m^{-1}}$.

According to Eq. (21) from Appendix A, the direct accelerance at TP1 of SH1 $h_{a,11}^{sh,1}$ may be synthesised as

$$h_{a,11}^{sh,1}(s) = \frac{a_0 s^2 + a_1 s + a_2}{b_0 s^2 + b_1 s + b_2} \tag{15}$$

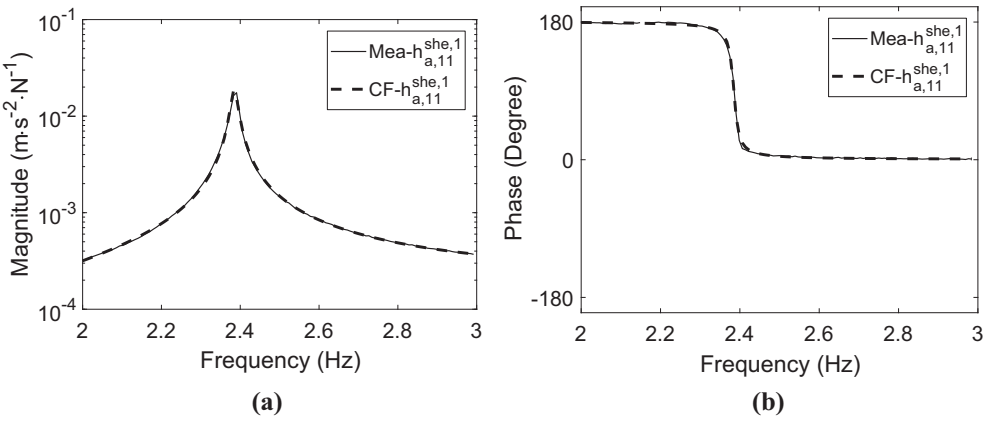

Fig. 14. Comparison between measured and curve-fitted accelerenaces $h_{a,11}^{she,1}$: (a) Magnitude; (b) Phase.

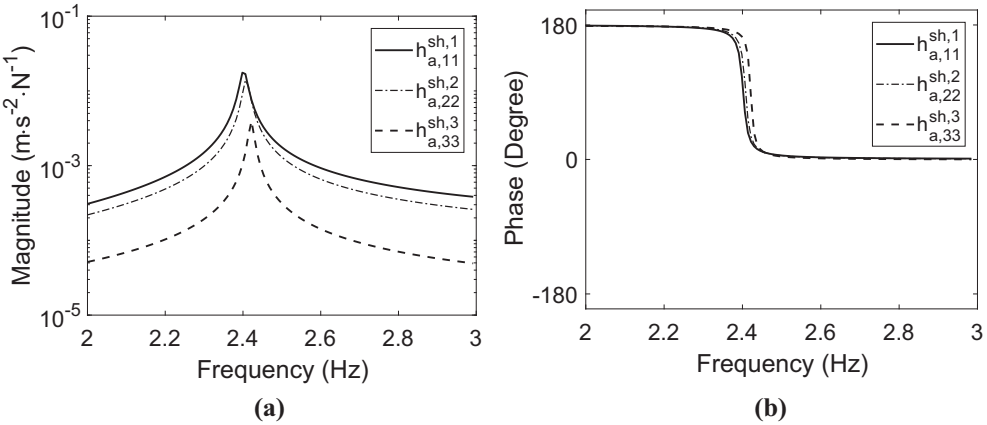

Fig. 15. Comparison of corrected $h_{a,11}^{sh,1}$, $h_{a,22}^{sh,2}$ and $h_{a,33}^{sh,3}$: (a) Magnitude; (b) Phase.

where $a_0 = 2.4765 \times 10^{-4}$, $a_1 = -1.2855 \times 10^{-5}\ \mathrm{s}^{-1}$, $a_2 = -1.6099 \times 10^{-5}\ \mathrm{s}^{-2}$, $b_0 = 1.8176\ \mathrm{N{\cdot}s^2{\cdot}m^{-1}}$, $b_1 = 0.1983\ \mathrm{N{\cdot}s{\cdot}m^{-1}}$ and $b_2 = 413.9403\ \mathrm{N{\cdot}m^{-1}}$.

Similarly, the accelerances $h_{a,22}^{sh,2}$, $h_{a,33}^{sh,3}$, $h_{a,31}^{sh,1}$ and $h_{a,13}^{sh,3}$ were synthesised. The corrected acelerances $h_{a,11}^{sh,1}$, $h_{a,22}^{sh,2}$ and $h_{a,33}^{sh,3}$ are shown in Fig. 15, in which the peak shift was induced by the presence of the human occupant at different locations only.

4.1.3. The identification of the dynamics of the human body and the empty structure

A pair of eigenvalues of the human-bridge system SH1 may be obtained as $\mu_{1,2}^{sh,1} = -0.0545 \pm 15.0910\mathrm{i}\ \mathrm{s}^{-1}$ by solving the characteristic equation of $h_{a,11}^{sh,1}$. Using $\mu_{1,2}^{sh,1}$ or the points around the minimum point in Fig. 16 as the initial guesses for the zeros of $\Delta h^{13}(s) = h_{a,11}^{sh,1}(s) - h_{a,33}^{sh,3}(s)$, a pair of eigenvalues may be obtained as $\mu_{1,2}^{s} = -0.0351 \pm 15.2338\mathrm{i}\ \mathrm{s}^{-1}$, which were also found to be zeros of $\Delta h^{12}(s)$ and $\Delta h^{23}(s)$. This confirms that $\mu_{1,2}^{s}$ were the eigenvalues of the empty bridge. The corresponding frequency and damping ratio were calculated to be 2.42 Hz and 0.23%, which agree well with the measured counterparts from impact hammer testing in which the hammer operator stood next to the bridge.

Based on the analytical expression of $h_{a,11}^{sh,1}$ given by Eq.(15), the identified eigenvalues of the empty bridge and the human mass ($m_h = 100$ kg), the damping and stiffness of the human body were calculated as

$$\begin{bmatrix} c_h \\ k_h \end{bmatrix} = \begin{bmatrix} \mu_1^s & 1 \\ \mu_2^s & 1 \end{bmatrix}^{-1} \begin{bmatrix} \frac{(\mu_1^s)^2 m_h}{m_h h_{a,11}^{sh,1}(\mu_1^s) - 1} \\ \frac{(\mu_2^s)^2 m_h}{m_h h_{a,11}^{sh,1}(\mu_2^s) - 1} \end{bmatrix} = \begin{bmatrix} 1.75 \times 10^3\ \mathrm{N{\cdot}s{\cdot}m^{-1}} \\ 7.21 \times 10^4\ \mathrm{N{\cdot}m^{-1}} \end{bmatrix} \tag{16}$$

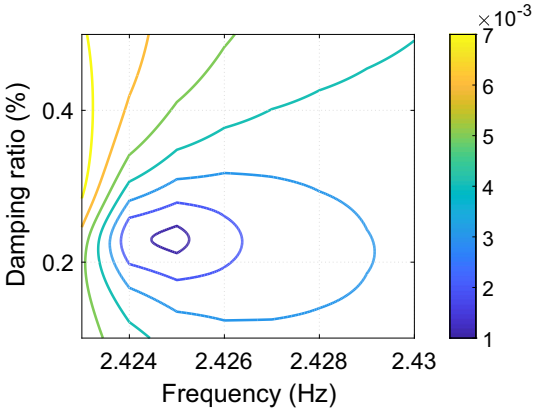

Fig. 16. The magnitude of $\Delta h^{13}(s)$ against frequency and damping ratio.

from which the corresponding frequency and damping ratio were calculated to be $f_h = 4.27$ Hz and $\zeta_h = 33\%$, respectively. These results are in the ranges of natural frequency and damping ratio for a human body in a standing posture availabe in the literature [20].

Based on the corrected accelerances $h^{sh,1}_{a,11}$, $h^{sh,2}_{a,22}$, $h^{sh,3}_{a,33}$, $h^{sh,1}_{a,31}$ and $h^{sh,3}_{a,13}$, the identified human body dynamics and Eqs. (1) and (2), the direct accelerances $h^{s}_{a,11}$, $h^{s}_{a,22}$ and $h^{s}_{a,33}$ and the cross accelerances $h^{s}_{a,13}$ and $h^{s}_{a,31}$ of the empty bridge can be synthesised, which are shown in Figs. 17 and 18. As can be seen from Fig. 17, the three direct accelerances of the empty bridge

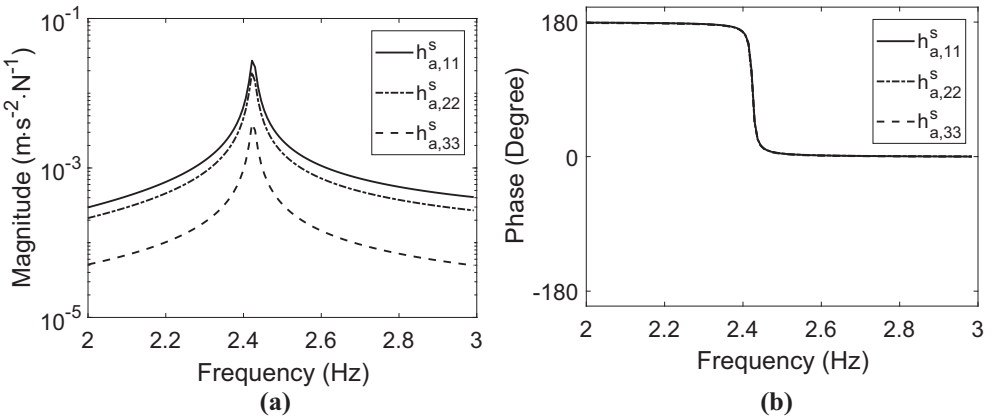

Fig. 17. Synthesised direct accelerances $h^{s}_{a,11}$, $h^{s}_{a,22}$ and $h^{s}_{a,33}$ of the empty bridge: (a) Magnitude; (b) Phase.

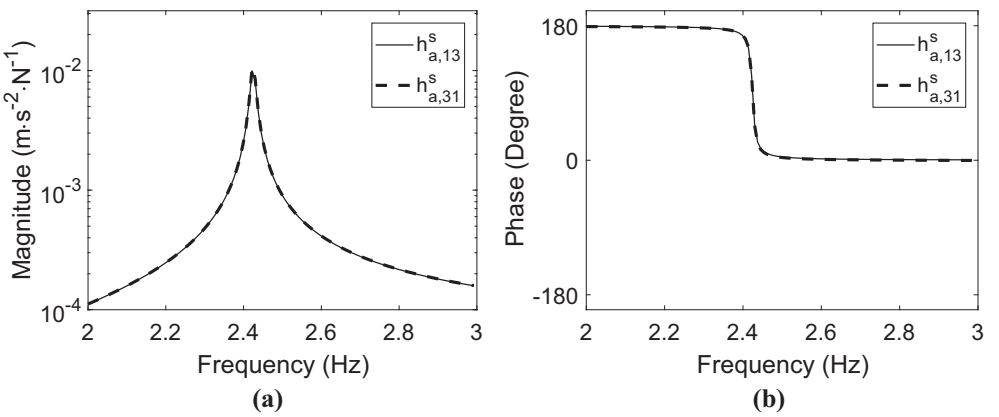

Fig. 18. Synthesised cross accelerances $h^{s}_{a,13}$ and $h^{s}_{a,31}$ of the empty bridge: (a) Magnitude; (b) Phase.

exhibit the same frequency. Fig. 18 implies that the principle of structural reciprocity is satisfied. In addition, the accelerances obtained by eliminating the effect of the shaker from the measured accelerances of the bridge with the shaker agree well with those obtained by eliminating the effects of the shaker and human occupant from the measured accelerances of the bridge with the human occupant and shaker. These suggest that the effects of the human occupant and shaker have been eliminated correctly.

4.2. The elimination of the effect of hammer operator in manually operated impact hammer testing

The same steel-concrete composite bridge used in Section 4.1 was considered again, but with 3.41 m overhang at each end, i.e. a span length of 13.08 m. The accelerances of the empty bridge and the hammer operator-bridge system were measured using manually operated impact hammer testing. The TPs are shown in Fig. 19.

4.2.1. Manually operated impact hammer testing

To obtain the accelerances of the empty bridge, the hammer operator stood next to the bridge to impact sequentially at TPs 1, 2 and 3 on the deck using an instrumented sledge hammer (Dytran Model 5803A, sensitivity 0.231 mV/N). Three accelerometers (Honeywell QA750, nominal sensitivity 1300 mV/g) were placed at TPs 1, 2 and 3 to measure the vibration responses of the empty bridge in the vertical direction. The data acquisition system consisted of a laptop, a 16-channel data logger (SignalCalc Mobilyser by Data Physics) and a signal conditioner. The sampling frequency was chosen to be 1024 Hz and the data acquisition window was set to 64 s. Four averages were used to minimise the effects of noise. No window was used since the vibration responses returned to the ambient vibration level at the end of the acquisition window. The accelerance measurement of the hammer operator-bridge system was performed in the same way. The only difference was that the hammer operator crouched on the deck (sequentially close to at TPs 1, 2 and 3) to perform the impact hammer testing. The typical crouching posture of the hammer operator is shown in Fig. 20. The hammer operator and the hammer weigh 62 kg and 5.5 kg, respectively. The bridge systems with the hammer operator crouching at TPs 1, 2 and 3 are designated as the systems SH1, SH2 and SH3, respectively.

The measured cross accelerances $h^s_{a,13}$ and $h^s_{a,31}$ of the empty bridge are compared in Fig. 21. It can be seen that the reciprocity holds for the empty bridge, which indicates that the dynamic behaviour of the bridge was linear in the response range of the tests. The bridge with the hammer operator crouching at TPs 1, 2 or 3 was also found to behave linearly by using

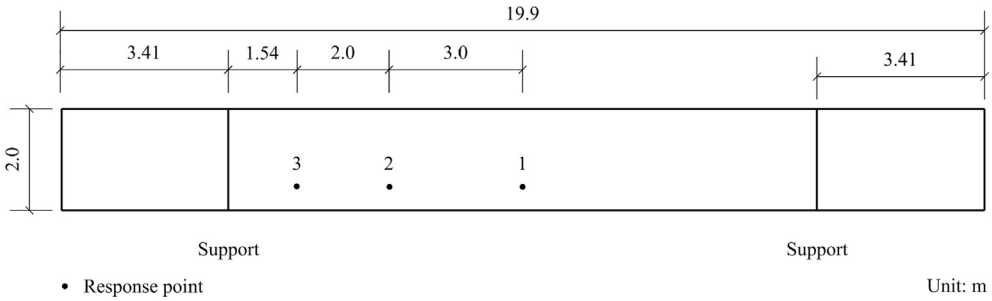

Fig. 19. Bridge deck geometry and test points.

Fig. 20. The bridge with the hammer operator crouching at TP2.

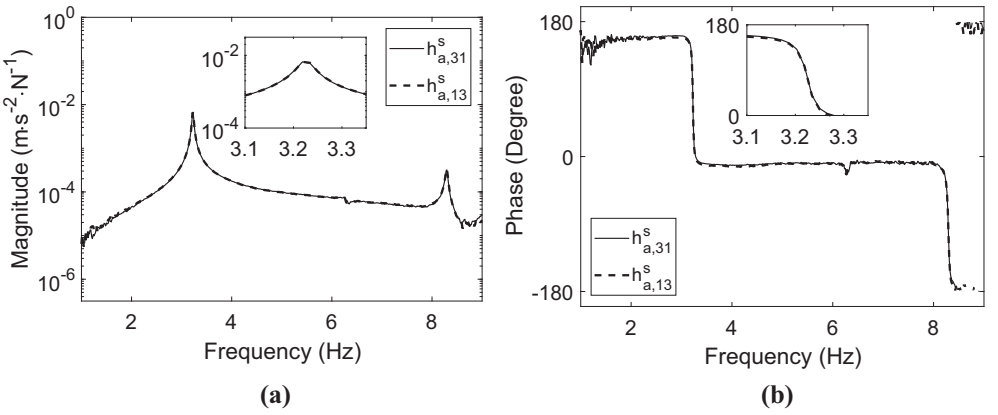

Fig. 21. Measured cross accelerances $h^{s}_{a,13}$ and $h^{s}_{a,31}$ of the empty bridge: (a) Magnitude; (b) Phase.

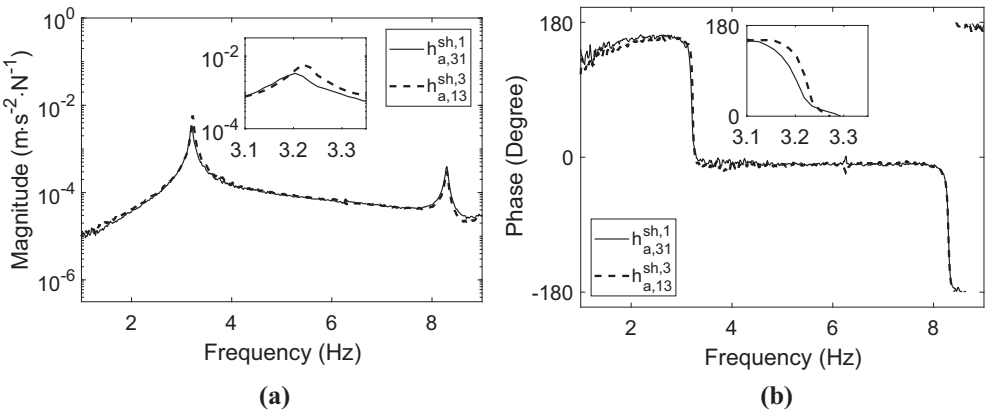

Fig. 22. Measured cross accelerances $h^{sh,1}_{a,31}$ and $h^{sh,3}_{a,13}$: (a) Magnitude; (b) Phase.

shaker testing. The response range of the shaker tests covers the range of the responses, bandpass filtered with cutoff frequencies 2 Hz and 6 Hz, of the impact hammer tests. Therefore, it is reasonable to assume that the dynamics of the hammer operator is linear during the testing. Fig. 22 shows that the cross accelerance $h^{sh,1}_{a,31}$ of the system SH1 did not agree with the cross accelerance $h^{sh,3}_{a,13}$ of the system SH3. This is due to the change in location of the hammer operator.

4.2.2. The elimination of the effect of the time delay of the measurement system

Fig. 21(b) and Fig. 22(b) shows that there was a phase shift at low frequencies (below 8 Hz) in the measured accelerances of the empty bridge and the hammer operator-bridge systems, indicating a time delay in the acceleration measurement compared to the impulse force measurement. By contrast, there was no time delay observed in the accelerance measurement in the shaker testing presented in Section 4.1.1. It is noted that three QA750 accelerometers were used for the response measurement in both the impact hammer testing and the shaker testing. While a load cell (an integral piezoelectric force sensor of low impedance voltage mode type) at the tip of the hammer Dytran Model 5803A was used for impulse force measurement, a QA750 accelerometer was used in the shaker testing to measure the excitation force. The time delay in the low frequency range in measured accelerances from the impact hammer testing was mainly due to the difference between the time constant of the load cell for force measurement and that of the accelerometer for response measurement [36]. In the shaker testing, these two time constants are equal, and therefore they do not affect measured accelerances [36]. Appendix B demonstrates that this time delay affects the estimation of actual accelerances of the system under test but not eigenvalues. The effect of the time delay must be corrected for accurate subsystem identification since the proposed theory for the dynamic identification of the human body (i.e. Eq. (9)) and the empty structure (i.e. Eqs. (1) and (2)) requires the estimation of actual accelerances of the human-structure system.

Eq. (26) in Appendix B shows that measured accelerances should be multiplied by $e^{\tau s}$, where τ (s) is the time delay of the measurement system. For the data acquisition system used in the impact hammer testing, an averaged time delay around the first mode may be approximately estimated as

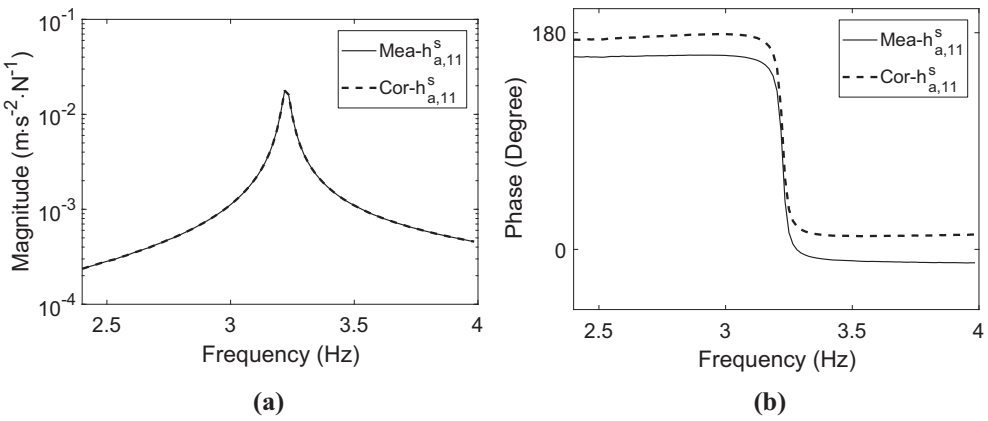

Fig. 23. Comparison of the measured accelerance $h^s_{a,11}$ and its phase corrected counterpart: (a) Magnitude; (b) Phase.

$$\tau = \frac{\theta}{360 f_1} \tag{17}$$

where θ (degree) is the averaged delayed phase angle and f_1 (Hz) is the natural frequency of the first mode. For example, the averaged delayed phase angle for the measured accelerance $h^s_{a,11}$ of the empty bridge was 19 degrees. The natural frequency was estimated to be 3.22 Hz. The time delay was calculated as 0.0164 s using Eq. (17). The comparison of the measured accelerance $h^s_{a,11}$ (thin solid line) and its phase corrected counterpart (thick dashed line) is displayed in Fig. 23. It can be seen that the phase has been corrected such that the phase angle is almost 180 degrees before the phase drop at the fundamental frequency, while there are no changes of the eigenvalues and magnitude of the FRF. In addition, it is reasonable to assume that all the measured accelerances had the same time delay since the same measurement system was used throughout the impact hammer testing.

4.2.3. The identification of the dynamics of the hammer operator and the empty bridge

After phase correction, the measured direct accelerance $h^{sh,1}_{a,11}$ was curve fitted around the first mode using the rational fraction polynomial method [35]. The estimated eigenvalues were $\mu^{sh,1}_{1,2} = -0.1930 \pm 20.0834\mathrm{i}\ \mathrm{s}^{-1}$ (the corresponding natural frequency and damping ratio were 3.20 Hz and 0.96%), and the corresponding analytical expression was

$$h^{sh,1}_{a,11}(s) = \frac{a_0 s^2 + a_1 s + a_2}{b_0 s^2 + b_1 s + b_2} \tag{18}$$

where $a_0 = 1.4493 \times 10^{-4}$, $a_1 = -3.1393 \times 10^{-4}\ \mathrm{s}^{-1}$, $a_2 = -0.0101\ \mathrm{s}^{-2}$, $b_0 = 1.1569\ \mathrm{N{\cdot}s^2{\cdot}m^{-1}}$, $b_1 = 0.4466\ \mathrm{N{\cdot}s{\cdot}m^{-1}}$ and $b_3 = 466.6605\ \mathrm{N{\cdot}m^{-1}}$.

Similarly, the phase corrected $h^{sh,3}_{a,33}$ was curved fitted and the eigenvalues were identified to be $\mu^{sh,3}_{1,2} = -0.1030 \pm 20.2371\mathrm{i}\ \mathrm{s}^{-1}$ (natural frequency and damping ratio were 3.22 Hz and 0.51%). Its analytical expression was

$$h^{sh,3}_{a,33}(s) = \frac{a_0 s^2 + a_1 s + a_2}{b_0 s^2 + b_1 s + b_2} \tag{19}$$

where $a_0 = 2.9953 \times 10^{-5}$, $a_1 = -1.1264 \times 10^{-4}\ \mathrm{s}^{-1}$, $a_2 = -0.0581\ \mathrm{s}^{-2}$, $b_0 = 8.0321\ \mathrm{N{\cdot}s^2{\cdot}m^{-1}}$, $b_1 = 1.6684\ \mathrm{N{\cdot}s{\cdot}m^{-1}}$ and $b_2 = 3289.7\ \mathrm{N{\cdot}m^{-1}}$.

With $\mu^{sh,3}_{1,2}$ or the points around the minimum point shown in Fig. 24 as the initial guesses, $\mu^s_{1,2} = -0.0868 \pm 20.2622\mathrm{i}\ \mathrm{s}^{-1}$ were found to be the common zeros of $\Delta h^{13}(s)$, $\Delta h^{12}(s)$ and $\Delta h^{23}(s)$, which confirms that $\mu^s_{1,2}$ were the eigenvalues of the empty bridge. The corresponding natural frequency and damping ratio of the empty bridge were found to be 3.22 Hz and 0.43%, which agree with those identified from accelerances directly measured on the empty bridge.

By using the eigenvalues $\mu^s_{1,2}$, $m_h = 62 + 5.5 = 67.5$ kg, Eq. (11) and Eq. (18), the human body dynamics were identified as

$$\begin{bmatrix} c_h \\ k_h \end{bmatrix} = \begin{bmatrix} \mu^s_1 & 1 \\ \mu^s_2 & 1 \end{bmatrix}^{-1} \begin{bmatrix} \frac{(\mu^s_1)^2 m_h}{m_h h^{sh,1}_{a,11}(\mu^s_1) - 1} \\ \frac{(\mu^s_2)^2 m_h}{m_h h^{sh,1}_{a,11}(\mu^s_2) - 1} \end{bmatrix} = \begin{bmatrix} 8.86 \times 10^2\ \mathrm{N{\cdot}s{\cdot}m^{-1}} \\ 3.71 \times 10^4\ \mathrm{N{\cdot}m^{-1}} \end{bmatrix} \tag{20}$$

from which the natural frequency and damping ratio of the human occupant operating a hammer in a crouching posture were calculated to be 3.73 Hz and 28%.

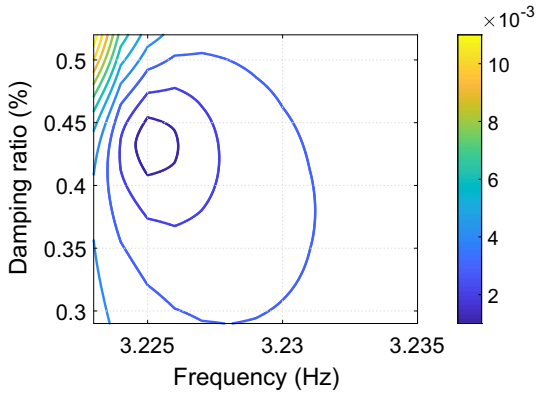

Fig. 24. The magnitude of $\Delta h^{13}(s)$ against frequency and damping ratio.

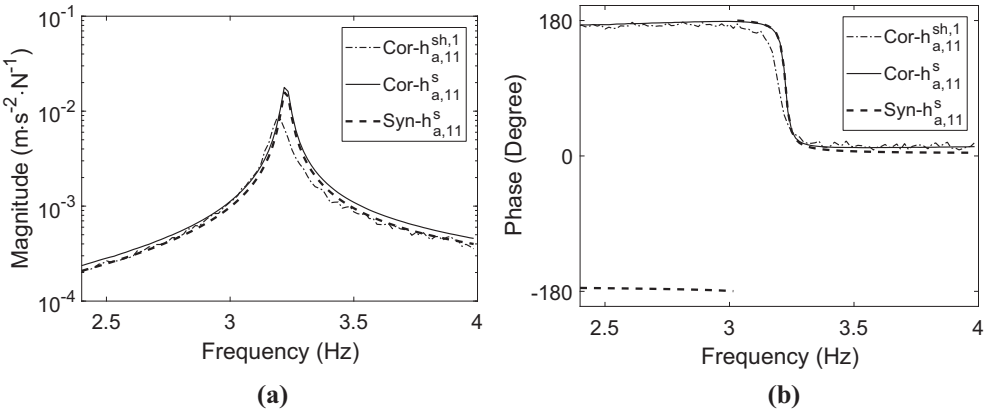

Fig. 25. Comparison of the synthesised accelerance of the empty bridge and the phase corrected accelerances measured on the empty bridge and the human-bridge system: (a) Magnitude; (b) Phase.

With the identified human body dynamics and the analytical expression of the phase corrected $h^{sh,1}_{a,11}(s)$ given by Eq. (18), Eq. (1) gives the direct accelerance at TP1 of the empty structure. Fig. 25 shows that the synthesised accelerance $h^{s}_{a,11}(s)$ (thick dashed line) agrees reasonably well with the measured counterpart of the empty bridge with phase corrected (thin solid line). The comparison of the identified frequencies and damping ratios of the hammer operator-bridge systems and the empty bridge indicates that the presence of the hammer operator causes the decrease of the natural frequency of the empty bridge and the increase of the damping ratio. This also explains the difference between the phase corrected accelerance of the hammer-operator system (thin dash-dotted line) and that of the empty bridge shown in Fig. 25. Similarly, other accelerances of the empty bridge can be synthesised by eliminating the effect of the hammer operator.

5. Conclusions

A novel method for subsystem identification in a human-structure system has been proposed. It enables the identification of the dynamic properties of the human body and the empty structure from measured FRFs of the human-structure system. The proposed theory is verified by a numerical example and two experimental case studies. The method is especially relevant to the elimination of the effect of the hammer operator in manually operated impact hammer testing on lightweight civil engineering structures. In addition, the method can be generalised to compensate for the effects of the shaker in shaker testing. Furthermore, the time delay between the force and response signals on the measured FRFs of the structure under test are discussed, and appropriate strategies for their correction are proposed. The proposed method, which focuses on the presence of a single human occupant on lightweight low-frequency structures (up to 8 Hz) in this paper, will be extended to the crowd-structure interaction in the future work.

Acknowledgment

This research was supported by the UK Engineering and Physical Sciences Research Council [grant number EP/M021505/1: Characterising dynamic performance of fibre reinforced polymer structures for resilience and sustainability].

Data availability

Electronic format of the data collected in this research can be downloaded freely from the University of Warwick webpages http://wrap.warwick.ac.uk/108822.

Appendix A. The elimination of the effect of shaker on measured FRFs of the empty structure

The method for the elimination of the effect of a human occupant on the dynamic identification of the empty structure presented in the paper [18] can be extended to the elimination of the effect of shaker on measured FRFs. Under the assumption that a shaker is a mass block of the total mass m_e, the resultant formulas are the same as those used for the elimination of transducer mass loading effects in some studies [37,38]. Hence, the derivation of the formulas is not presented here, instead they are shown in the final form.

Namely, the direct receptance at the p-th DOF ($p \leq n$) of the empty structure $h^s_{pp}(s)$ and that of the structure with the shaker at the p-th DOF $h^{se,p}_{pp}(s)$ are related by

$$h^s_{pp}(s) = \frac{h^{se,p}_{pp}(s)}{1 - m_e s^2 h^{se,p}_{pp}(s)} \tag{21}$$

Similarly, the cross receptance between the q-th DOF ($p \leq n$) and the p-th DOF of the empty structure $h^s_{qp}(s)$ and that of the structure with the shaker at the p-th DOF $h^{se,p}_{qp}(s)$ are related by

$$h^s_{qp}(s) = \frac{h^{se,p}_{qp}(s)}{1 - m_e s^2 h^{se,p}_{qp}(s)} \tag{22}$$

Appendix B. The effect of the time delay of the measurement system on measured FRFs

The equation of forced vibration of a linear structure having n DOFs may be written in the Laplace domain as

$$\boldsymbol{x}_s(s) = \boldsymbol{H}_s(s)\boldsymbol{f}_s(s) \tag{23}$$

where $\boldsymbol{H}_s(s)$ is the receptance matrix, s is the Laplace variable, whilst $\boldsymbol{x}_s(s)$ and $\boldsymbol{f}_s(s)$ are the Laplace transforms of displacement and force vectors.

In the modal testing of the above system, if the measurement system is an ideal system but there is a time delay, τ, between the response and force signal measurement, then the measurement system FRF can be expressed as $e^{-\tau s}$. The equation of forced vibration of the structure combined with the measurement system then becomes

$$\tilde{\boldsymbol{x}}_s(s) = \boldsymbol{H}_s(s)e^{-\tau s}\boldsymbol{f}_s(s) \tag{24}$$

where $\tilde{\boldsymbol{x}}_s(s)$ is the Laplace transform of the measured output of the structure combined with the measurement system.

The measured receptance then becomes

$$\tilde{\boldsymbol{H}}_s(s) = \frac{\tilde{\boldsymbol{x}}_s(s)}{\boldsymbol{f}_s(s)} = \boldsymbol{H}_s(s)e^{-\tau s} \tag{25}$$

which shows that the actual receptance of the structure may be obtained by correcting the measured receptance by

$$\boldsymbol{H}_s(s) = \tilde{\boldsymbol{H}}_s(s)e^{\tau s} \tag{26}$$

References

[1] B.R. Ellis, T. Ji, Human-structure interaction in vertical vibrations, Proc. Inst. Civ. Eng. Struct. Build. 122 (1997) 1–9.
[2] R. Sachse, A. Pavic, P. Reynolds, Parametric study of modal properties of damped two-degree-of-freedom crowd–structure dynamic systems, J. Sound Vib. 274 (2004) 461–480.
[3] J.M.W. Brownjohn, Energy dissipation from vibrating floor slabs due to human-structure interaction, Shock Vib. 8 (2001).
[4] S. Živanović, I. Diaz, A. Pavić, Influence of walking and standing crowds on structural dynamic properties, Proceeding of Conference & Exposition on Structural Dynamics (IMAC XXVII), 2009.
[5] J. Sim, Human-structure interaction in cantilever grandstands (Ph.D. Thesis), The University of Oxford, 2006.
[6] R. Sachse, A. Pavic, P. Reynolds, Human-structure dynamic interaction in civil engineering dynamics: a literature review, Shock Vib. Digest 35 (2003) 3–18.
[7] S. Živanović, A. Pavic, P. Reynolds, Vibration serviceability of footbridges under human-induced excitation: a literature review, J. Sound Vib. 279 (2005) 1–74.
[8] S. Živanović, G. Feltrin, J.T. Mottram, J.M.W. Brownjohn, Vibration performance of bridges made of fibre reinforced polymer, in: F.N. Catbas (Ed.), Dynamics of Civil Structures, Volume 4: Proceedings of the 32nd IMAC, A Conference and Exposition on Structural Dynamics, 2014, Springer International Publishing, Cham, 2014, pp. 155–162.

[9] E. Shahabpoor, A. Pavic, V. Racic, Interaction between walking humans and structures in vertical direction: a literature review, Shock Vib. 2016 (2016) 22.
[10] R.O. Foschi, G.A. Neumann, F. Yao, B. Folz, Floor vibration due to occupants and reliability-based design guidelines, Can. J. Civ. Eng. 22 (1995) 471–479.
[11] Y. Matsumoto, M.J. Griffin, Dynamic response of the standing human body exposed to vertical vibration: influence of posture and vibration magnitude, J. Sound Vib. 212 (1998) 85–107.
[12] L. Wei, M.J. Griffin, Mathematical models for the apparent mass of the seated human body exposed to vertical vibration, J. Sound Vib. 212 (1998) 855–874.
[13] X. Zheng, J.M.W. Brownjohn, Modeling and simulation of human-floor system under vertical vibration, in: L.P. Davis (Ed.), Proc. SPIE 4327, Smart Structures and Materials 2001: Smart Structures and Integrated Systems, Newport Beach, CA, USA, 2001, pp. 513–520.
[14] R. Sachse, The influences of human occupants on the dynamic properties of slender structures (Ph.D. Thesis), University of Sheffield, 2003.
[15] K. Van Nimmen, K. Maes, S. Zivanovic, G. Lombaert, G. De Roeck, P. Van den Broeck, Identification and modelling of vertical human-structure interaction, in: J. Caicedo, S. Pakzad (Eds.), Dynamics of Civil Structures, Volume 2: Proceedings of the 33rd IMAC, A Conference and Exposition on Structural Dynamics, 2015, Springer International Publishing, Cham, 2015, pp. 319–330.
[16] E. Shahabpoor, A. Pavic, V. Racic, Identification of mass–spring–damper model of walking humans, Structures 5 (2016) 233–246.
[17] E. Shahabpoor, A. Pavic, V. Racic, Identification of walking human model using agent-based modelling, Mech. Syst. Sig. Process. 103 (2018) 352–367.
[18] X. Wei, S. Živanović, Frequency response function-based explicit framework for dynamic identification in human-structure systems, J. Sound Vib. 422 (2018) 453–470.
[19] J. Sim, A. Blakeborough, M. Williams, Modelling effects of passive crowds on grandstand vibration, Proc. Inst. Civ. Eng. Struct. Build. 159 (2006) 261–272.
[20] C.A. Jones, P. Reynolds, A. Pavic, Vibration serviceability of stadia structures subjected to dynamic crowd loads: a literature review, J. Sound Vib. 330 (2011) 1531–1566.
[21] C.C. Caprani, E. Ahmadi, Formulation of human–structure interaction system models for vertical vibration, J. Sound Vib. 377 (2016) 346–367.
[22] J.W. Qin, S.S. Law, Q.S. Yang, N. Yang, Finite element analysis of pedestrian-bridge dynamic interaction, J. Appl. Mech. 81 (2013), 041001-041001-041015.
[23] A. Pavic, R. Pimentel, P. Waldron, Instrumented sledge hammer impact excitation: worked examples, in: Proceedings-Spie the International Society for Optical Engineering, Spie The International Socienty for Optica, 1998, pp. 929–935.
[24] D. Tirelli, Modal Analysis of Small & Medium Structures by Fast Impact Hammer Testing Method, 2011.
[25] S. Živanović, X. Wei, J. Russell, J.T. Mottram, Vibration performance of two FRP footbridge structures in the United Kingdom, in: Footbridge 2017, Berlin, Germany, 2017.
[26] M.G.R. Toward, M.J. Griffin, Apparent mass of the human body in the vertical direction: inter-subject variability, J. Sound Vib. 330 (2011) 827–841.
[27] Y. Matsumoto, M.J. Griffin, Mathematical models for the apparent masses of standing subjects exposed to vertical whole-body vibration, J. Sound Vib. 260 (2003) 431–451.
[28] IStructE/DTLR/DCMS, Dynamic Performance Requirements for Permanent Grandstands Subject to Crowd Action, Recommendations for Management, Design and Assessment, The Institution of Structural Engineers (IStructE), London, 2008.
[29] A. Pavic, P. Reynolds, Experimental verification of novel 3DOF model for grandstand crowdstructure dynamic interaction, in: 26th International Modal Analysis Conference: IMAC-XXVI, Orlando, Florida, 2008.
[30] C.A. Jones, A. Pavic, P. Reynolds, R.E. Harrison, Verification of equivalent mass-spring-damper models for crowd-structure vibration response prediction, Can. J. Civ. Eng. 38 (2011) 1122–1135.
[31] K.A. Salyards, N.C. Noss, Experimental evaluation of the influence of human-structure interaction for vibration serviceability, J. Perform. Constr. Facil 28 (2014) 458–465.
[32] T. Coleman, Y. Li, An interior trust region approach for nonlinear minimization subject to bounds, SIAM J. Optim. 6 (1996) 418–445.
[33] ISO, ISO 5982:1981 Vibration and Shock – Mechanical Driving Point Impedance of the Human Body, International Organisation for Standarisation (ISO), Geneva, Switzerland, 1981.
[34] Z. Friedman, J.B. Kosmatka, An improved two-node Timoshenko beam finite element, Comput. Struct. 47 (1993) 473–481.
[35] M.H. Richardson, D.L. Formenti, Parameter estimation from frequency response measurements using rational fraction polynomials, in: The 1st Internation Modal Analysis Conference, Orlando, FL, 1982.
[36] K.G. McConnell, P.S. Varoto, Vibration Testing: Theory and Practice, Wiley, New Jersey, 2008.
[37] J.M.M. Silva, N.M.M. Maia, A.M.R. Ribeiro, Cancellation of mass-loading effects of transducers and evaluation of unmeasured frequency response functions, J. Sound Vib. 236 (2000) 761–779.
[38] O. Cakar, K.Y. Sanliturk, Elimination of transducer mass loading effects from frequency response functions, Mech. Syst. Sig. Process. 19 (2005) 87–104.